Molecular mechanisms of acetyltransferase/histone deacetylase involvement in high mobility group box 1 nucleoplasmic translocation in sepsis: A bioinformatics and experimental approach

WAN CHEN[1*], HUAN ZHAO[2*], YU CAO[2*], YUANYUAN ZHOU[2], PINGPING HU[1], CHAOWEN WU[1], YANLI ZHONG[1], WEI DENG[1], DENG XIANG[3], WENKUI SUN[2] and JIANLIN CHEN[2]

[1]Department of Critical Care Medicine, Xindu People's Hospital of Chengdu, Chengdu, Sichuan 610500, P.R. China; [2]Department of Transfusion Medicine, School of Laboratory Medicine, Key Laboratory of Target Discovery and Protein Drug Development in Major Diseases of Sichuan Higher Education Institutes, Key Laboratory of Sichuan Province for Specific Structure of Small Molecule Drugs, Clinical IVD Joint Research Center of Chengdu Medical College-Maccura Biotechnology, Chengdu Medical College, Chengdu, Sichuan 610500, P.R. China; [3]Department of Orthopedics, The First Affiliated Hospital of Chengdu Medical College, Chengdu, Sichuan 610500, P.R. China

Received December 16, 2025; Accepted September 2, 2026

DOI: 10.3892/etm.2026.13350

Abstract. High mobility group box 1 (HMGB1) nuclear-cytoplasmic translocation is a key event in sepsis-associated inflammation, but the upstream mechanisms regulating this process remain incompletely understood. The present study aimed to investigate the associations among C-X-C motif chemokine ligand 8 (CXCL8)-PI3K/Akt signaling in HMGB1 nuclear-cytoplasmic translocation and to examine concurrent acetyltransferase (HAT)/histone deacetylase (HDAC)-associated changes under inflammatory conditions. RAW264.7 macrophages were stimulated with lipopolysaccharide (LPS) to induce septic conditions and HMGB1 subcellular localization was assessed using western blotting. In addition, HAT and HDAC enzymatic activities were measured using colorimetric activity assay kits. Bioinformatics analysis of sepsis-associated datasets (GSE46955 and GSE57065) identified CXCL8 as a hypothesis-generating candidate core gene. In an LPS/IFN-γ-induced THP-1-derived inflammatory macrophage model, HMGB1 nuclear-cytoplasmic translocation was also observed, together with increased CXCL8, CREB-binding protein and p300 mRNA levels, decreased HDAC1, HDAC2 and HDAC4 mRNA levels and activated Akt phosphorylation at Ser473. Representative western blotting results following treatment with the C-X-C motif chemokine receptor (CXCR)1/2 inhibitor Reparixin or the PI3K inhibitor LY294002 provided preliminary support for the potential involvement of CXCR1/2-PI3K/Akt signaling in HMGB1 nuclear-cytoplasmic translocation. Collectively, these findings support a potential role for CXCL8/CXCR1/2-PI3K/Akt signaling in HMGB1 nuclear-cytoplasmic translocation and provide complementary, hypothesis-generating evidence associating HAT/HDAC-related changes to this process.

Correspondence to: Dr Wenkui Sun or Professor Jianlin Chen, Department of Transfusion Medicine, School of Laboratory Medicine, Key Laboratory of Target Discovery and Protein Drug Development in Major Diseases of Sichuan Higher Education Institutes, Key Laboratory of Sichuan Province for Specific Structure of Small Molecule Drugs, Clinical IVD Joint Research Center of Chengdu Medical College-Maccura Biotechnology, Chengdu Medical College, 783 Xindu Avenue, Chengdu, Sichuan 610500, P.R. China
E-mail: sunwenkui126@126.com
E-mail: chenjianlin@cmc.edu.cn

*Contributed equally

Key words: high mobility group box 1, sepsis, nuclear-cytoplasmic translocation, C-X-C motif chemokine ligand 8, PI3K/Akt

Introduction

Sepsis, characterized by organ dysfunction resulting from a dysregulated immune response to infection, presents a notable challenge in critical care medicine (1). It is estimated that ~50 million cases of sepsis and ~11 million sepsis-associated mortalities are reported annually, constituting ~19.7% of global mortalities (2-4). In China alone, the annual hospitalization range for sepsis cases is 4.8-6.1 million, with a mortality rate of ~13.1% (5). Despite advances in its recognition and management, sepsis remains a key cause of morbidity and mortality worldwide (4), necessitating further research to elucidate its complex pathogenic mechanisms and identify effective therapeutic targets.

Previous research has investigated the molecular mechanisms of sepsis, with results indicating that high mobility group box 1 (HMGB1) serves a key role in the inflammatory process (6,7). HMGB1 is a ubiquitous and evolutionarily conserved non-histone

chromatin-binding protein. In the nucleus, HMGB1 functions as a DNA chaperone and chromatin-associated architectural factor involved in chromatin organization and a number of DNA-dependent processes, including gene transcription, DNA replication, recombination and repair, as well as the maintenance of genomic stability (8,9). Furthermore, the subcellular location of HMGB1 is key to its function (10), as under normal conditions, HMGB1 predominantly resides in the nucleus. Yet, during infection and inflammation, it can translocate from the nucleus to the cytoplasm and subsequently undergo active secretion (11,12). This transition of HMGB1 from the nucleus to the cytoplasm represents a key early step in the active secretion of HMGB1, and its dysregulation is implicated in the pathogenesis of sepsis (13). Unlike early inflammatory mediators such as TNF or IL-1, HMGB1 is secreted later and sustains its release for an extended period, aligning with key time points in sepsis-associated mortalities (14-18). Administration of antibodies or inhibitors against HMGB1 during these periods has been shown to markedly reduce mortality rates from endotoxemia or sepsis (14,17), emphasizing the key role of HMGB1 as a major late inflammatory mediator in the pathological process of sepsis (13). However, the specific mechanisms underlying HMGB1 nuclear-cytoplasmic translocation remain poorly understood.

Previous findings have indicated that acetyltransferase (HAT) and histone deacetylase (HDAC)-associated enzymes may influence HMGB1 nuclear-cytoplasmic translocation (19,20). Sirtuin 1, a member of the class III histone deacetylase family, has been reported to favor the nuclear retention of HMGB1 and limit its nuclear-cytoplasmic translocation (20). By contrast, p300 promotes the translocation of HMGB1 from the nucleus to the cytoplasm (21). These findings suggest that HAT/HDAC-associated regulation may influence HMGB1 subcellular distribution by modulating its acetylation status. Acetylation mediated by the HATs p300 and KAT2B promotes HMGB1 translocation from the nucleus to the cytoplasm, whereas SIRT1-mediated deacetylation favors HMGB1 nuclear retention and inhibits its nuclear-cytoplasmic translocation. However, the signaling mechanisms associated with this process remain unclear.

The PI3K/Akt signaling pathway modulates macrophage responses to inflammatory and microbial stimuli (22,23). Previous evidence has demonstrated that pharmacological suppression of PI3K signaling reduced lipopolysaccharide (LPS)-induced HMGB1 nuclear-cytoplasmic translocation and secretion (24). Despite this, the direct involvement of Akt in HMGB1 nuclear-cytoplasmic translocation remains unclear. C-X-C motif chemokine ligand 8 (CXCL8) is a key inflammatory chemokine that signals primarily through C-X-C motif chemokine receptor (CXCR)-1 and CXCR2 and contributes to leukocyte recruitment and inflammatory responses (25,26). In intrahepatic cholangiocarcinoma cells, CXCL8 has been shown to activate PI3K/Akt signaling through CXCR2 (27). However, whether CXCL8-associated signaling and PI3K/Akt activation contribute to HMGB1 nuclear-cytoplasmic translocation during sepsis-associated inflammation has not been established. Therefore, the present study combined bioinformatics screening with pharmacological experiments to investigate the potential involvement of CXCL8-PI3K/Akt signaling in HMGB1 nuclear-cytoplasmic translocation. HAT- and HDAC-associated changes were also examined to characterize the molecular events accompanying HMGB1 redistribution.

Materials and methods

Cell culture and inflammatory model construction. As a murine macrophage cell line, RAW264.7 (purchased from the Research and Experimental Center of Chengdu Medical College) was cultivated in DMEM medium (cat. no. PM150210; Procell Biotechnology Co., Ltd.) supplemented with 10% FBS (cat. no. 164210; Pricella Biotechnology Co., Ltd.) and 1% penicillin/streptomycin at 37˚C with 5% CO_2. Upon reaching 60-70% density, cells were seeded at $5x10^6$ cells per well in 6-well plates. Upon achieving ~80% confluence, nuclear and cytoplasmic proteins were extracted following stimulation with 100 ng/ml LPS from *Escherichia coli* O111:B4 (cat. no. L4391; Sigma-Aldrich; Merck KGaA) for 6, 8, 10, 12, 14 or 16 h, whereas untreated cells collected at 0 h served as the control. Following the indicated treatments, nuclear and cytoplasmic protein fractions were isolated using a Nuclear and Cytoplasmic Protein Extraction Kit (cat. no. P0028; Beyotime Biotechnology), as described in the following subsection.

The human monocyte THP-1 cell line, purchased from Procell Life Science & Technology Co., Ltd., was maintained in RPMI-1640 medium (cat. no. PM150110; Procell Biotechnology Co., Ltd.) supplemented with 10% FBS, 0.05 mM β-mercaptoethanol and 1% penicillin/streptomycin at 37˚C with 5% CO_2. Cells were plated at a density of $1x10^6$ cells per well in 6-well plates.

Optimization of PMA-induced THP-1 cell differentiation. To optimize phorbol 12-myristate 13-acetate (PMA)-induced differentiation, THP-1 cells were seeded into 6-well plates at a density of $1x10^6$ cells/well in 2 ml complete culture medium. Following incubation for 24 h, the cells were treated with 30, 100 or 200 ng/ml PMA (cat. no. HY-18739; MedChemExpress) for an additional 24 h. Cellular adherence, spreading, cytoplasmic protrusion formation and macrophage-like morphological changes were examined using an inverted light microscope at x100 and x200 magnification. The PMA concentration range and 24-h treatment period were informed by a previously published THP-1 differentiation study (28).

Based on the optimization results, THP-1 cells differentiated with 100 ng/ml PMA for 24 h were used for subsequent experiments. To establish an inflammatory macrophage model, PMA-differentiated cells were stimulated with 100 ng/ml LPS and 20 ng/ml IFN-γ (cat. no. 300-02; PeproTech, Inc.; Thermo Fisher Scientific, Inc.). These concentrations were selected according to an established THP-1 inflammatory macrophage-model protocol (29). Cells were collected at 6, 8, 10, 12, 14 and 16 h for the time-course analysis of HMGB1 nuclear-cytoplasmic translocation. PMA-differentiated cells collected immediately before LPS/IFN-γ stimulation served as the 0 h control. To validate the inflammatory macrophage model, the mRNA expression levels of TNF-α, IL-1β and IL-6 were measured using reverse transcription-quantitative PCR (RT-qPCR) after 10 h of stimulation.

Cell viability under inflammatory stimulation conditions. Cell viability was assessed using a Cell Counting Kit-8 assay

(CCK-8; cat. no. BS350A; Biosharp Life Sciences). THP-1 cells were seeded into 96-well plates at $2x10^4$ cells/well and differentiated with 100 ng/ml PMA for 24 h at 37˚C with 5% CO_2, followed by stimulation with 100 ng/ml LPS and 20 ng/ml IFN-γ for 10, 12, 14 or 16 h at 37˚C with 5% CO_2. RAW264.7 cells were seeded at $2.5x10^4$ cells/well and stimulated with 100 ng/ml LPS for the same durations at 37˚C with 5% CO_2. Each condition was tested in triplicate. Subsequently, 10 μl CCK-8 reagent was added to each well and incubated for 1 h at 37˚C. Absorbance was measured at 450 nm and cell viability was calculated relative to the untreated control group.

Protein extraction for nuclear, cytoplasmic and total cellular fractions. Nuclear and cytoplasmic proteins were extracted using a Nuclear and Cytoplasmic Protein Extraction Kit (cat. no. P0028; Beyotime Biotechnology) following the manufacturer's instructions. The harvested cells were treated with cytoplasmic protein extraction reagent A containing PMSF (cat. no. ST507; Beyotime Biotechnology), vigorously vortexed for 5 sec and then incubated in an ice bath for 10 min. Subsequently, reagent B was added to the suspension, followed by vigorous vortexing for 5 sec and an additional ice bath incubation for 1 min. After a 5 sec vortex and centrifugation at 12,000-16,000 x g for 5 min at 4˚C, the supernatant was collected as cytoplasmic proteins. The remaining precipitate was subjected to nuclear protein extraction using a reagent containing PMSF. The supernatant fraction, containing nuclear proteins, was collected after repeated vigorous vortexing and a 30 min ice bath, followed by centrifugation at 12,000-16,000 x g for 10 min at 4˚C. Total cellular proteins were obtained by lysing the cells with 1X RIPA lysis buffer (cat. no. AR0102-10; Boster Biological Technology) supplemented with 1% PMSF and 1% phosphatase inhibitor for subsequent experiments.

Assessment of HAT and HDAC enzyme activity. HAT enzymatic activity was measured using a HAT Activity Colorimetric Assay Kit (cat. no. K332-100; BioVision, Inc.; Abcam) according to the manufacturer's instructions. Briefly, nuclear protein samples were prepared at 50 μg per reaction in 40 μl double-distilled water (ddH_2O) in a 96-well plate. For background controls, 40 μl ddH_2O was added instead of sample. For each reaction, 68 μl freshly prepared assay mixture, containing 2X HAT assay buffer, HAT substrate I, HAT substrate II and nicotinamide adenine dinucleotide-generating enzyme, was added to initiate the reaction. The plate was incubated at 37˚C for 1-4 h depending on color development and absorbance was measured at 440 nm using a microplate reader. Background absorbance from wells without HAT-containing sample was subtracted from all sample readings. HAT activity was expressed as the relative optical density (OD) 440 value normalized to protein amount or as fold change relative to the control group. HDAC enzymatic activity was measured using a HDAC Activity Colorimetric Assay Kit (cat. no. K331-100; BioVision, Inc.; Abcam) according to the manufacturer's instructions. Briefly, nuclear extract or cell lysate samples were diluted to 85 μl ddH_2O per well. Subsequently, 10 μl 10X HDAC assay buffer and 5 μl HDAC colorimetric substrate were added to each well, followed by incubation at 37˚C for 1 h. The reaction was stopped by adding 10 μl lysine developer and the plate was further incubated at 37˚C for 30 min. Absorbance was measured at 400 or 405 nm using a microplate reader. Background absorbance was subtracted, and HDAC activity was expressed as the relative OD value normalized to protein amount or as fold change relative to the control group.

Source of sepsis and septic shock gene expression data. The gene expression microarray datasets GSE46955 and GSE57065, originally generated and reported by Shalova *et al* (30) and Cazalis *et al* (31), respectively, were obtained from the Gene Expression Omnibus (GEO) database (https://www.ncbi.nlm.nih.gov/geo/). These datasets comprise transcriptome analysis data from mononuclear cell samples of 8 patients with untreated sepsis and 6 healthy volunteers. In addition, the datasets include whole-genome information from blood samples of patients with septic shock within 30 min of shock onset, along with data from 25 healthy controls. Utilizing the 'ggplot2' package (32) (version 3.3.6) in R software (version 4.2.1; Posit Software, PBC), data visualization and analysis was performed.

Differential expression analysis in sepsis or septic shock. Series Matrix files and corresponding GPL platform annotation files were downloaded for each GEO dataset, including GPL6104 for GSE46955 and GPL570 for GSE57065. Employing the 'limma' R package (33) (version 3.52.2) through the GEO2R online analysis platform (https://www.ncbi.nlm.nih.gov/geo/geo2r/), differential expression analysis was performed. Genes with an adjusted $P<0.05$ and $\log_2$ fold change (FC) >1 were considered differentially expressed (DEGs). Visualization of DEGs was accomplished using the 'ggplot2' R package (version 3.3.6), while bidirectional cluster analysis was performed with the 'ComplexHeatmap' package (34) (version 2.13.1).

Gene Ontology (GO) and Kyoto Encyclopedia of Genes and Genomes (KEGG) enrichment analysis. Intersection of DEGs in GSE46955 and GSE57065 was determined using jvenn (version 1.8.1; http://www.bioinformatics.com.cn). The 'clusterProfiler' package (35) (version 4.6.2) in R software was employed to dissect the functions of these DEGs. Enrichment analysis was performed for GO and KEGG pathways. The top 10 ranked GO bar graphs, covering biological process, cellular component and molecular function, were generated based on a significance threshold of adjusted $P<0.05$. In addition, a KEGG pathway bubble diagram was constructed.

Identification of HAT and HDAC-associated gene targets. GeneCards (https://www.genecards.org/) was utilized to search for gene targets associated with HAT and HDAC. The category was set to 'Protein Coding' and the targets were filtered with a relevance score ≥ average. Duplicate values were removed, resulting in a list of relevant gene targets for HAT and HDAC.

Core gene identification and receiver operating characteristic (ROC) curve analysis. Overlapping targets were input into the Search Tool for the Retrieval of Interacting Genes/Proteins (STRING) data analysis platform (https://cn.string-db.org/) to obtain protein-protein interaction (PPI) data. After selecting

Table I. Primer sequences for reverse transcription-quantitative PCR.

Gene	Forward sequence (5'-3')	Reverse sequence (5'-3')
TNF-α	CCTCTCTCTAATCAGCCCTCTG	GAGGACCTGGGAGTAGATGAG
IL-1β	TACCTGTCCTGCGTGTTGAA	TGCTTGAGAGGTGCTGATGT
IL-6	CAATAACCACCCCTGAC	GCTACATTTGCCGAAGA
CXCL8	TTTTGCCAAGGAGTGCTAAAGA	AACCCTCTGCACCCAGTTTTC
CBP	CGGCTCTAGTATCAACCCAGG	TTTTGTGCTTGCGGATTCAGT
p300	TTGTGAAGAGCCCCATGGAT	GCTTTGCATCACTGGGTCAA
HDAC1	CGCCCTCACAAAGCCAATG	CTGCTTGCTGTACTCCGACA
HDAC2	ATGGCGTACAGTCAAGGAGG	TGCGGATTCTATGAGGCTTCA
HDAC3	GCAAGGCTTCACCAAGAGTCT	AGATGCGCCTGTGTAACGC
HDAC4	GGCCCACCGGAATCTGAAC	GAACTCTGGTCAAGGGAACTG
GAPDH	CAGGAGGCATTGCTGATGAT	GAAGGCTGGGGCTCATTT

CXCL8, C-X-C motif chemokine ligand 8; HDAC, histone deacetylase; CBP, CREB-binding protein.

'Homo sapiens' and removing unrelated nodes, the resulting tab-separated values file was exported for constructing the PPI network using Cytoscape (36) (version 3.9.0) software. Key genes were identified using the CytoNCA algorithm, with the core genes determined by intersecting key genes with those associated with HAT and HDAC. The discriminatory performance of the identified core gene was assessed using ROC one-factor analysis using the 'pROC' package (37) (version 1.18.0). GSE28750 was used as an external validation dataset and GSE69528 was included as an additional independent validation dataset to provide further exploratory support for the relevance of CXCL8. ROC curve analysis was performed separately within each dataset and the datasets were not pooled or merged for analysis. As the GEO datasets differed in sample type, disease-associated context, cohort structure and microarray platform, no cross-platform batch-effect correction was performed. The area under the curve (AUC) values were interpreted as measures of within-dataset discriminatory performance rather than as evidence of clinically validated diagnostic utility. The sample characteristics, disease-associated context, cohort structure, platform information and preprocessing or normalization procedures of each GEO dataset are summarized in Table SI.

RNA extraction and RT-qPCR analysis. Total RNA was extracted from THP-1-derived macrophages following the indicated treatments using TRIzol® reagent (cat. no. 15596026; Invitrogen; Thermo Fisher Scientific, Inc.). For reverse transcription, 1 μg total RNA was used for each reaction. Briefly, the reverse transcription reaction was prepared in a final volume of 20 μl, containing 4 μl of 5X ABScript III RT Mix, 1 μl of 20X gDNA Remover Mix, 1 μg total RNA template and nuclease-free water to 20 μl, using the ABScript III RT Master Mix Reverse Transcriber Kit (cat. no. RK20429; ABclonal Biotech Co., Ltd.). Reverse transcription was performed according to the manufacturer's instructions at 37˚C for 2 min, 55˚C for 15 min and 85˚C for 5 min, followed by maintenance at 4˚C. qPCR was performed using Genius 2X SYBR Green Fast qPCR Mix (No ROX; cat. no. RK21205; ABclonal Biotech Co., Ltd.). The thermocycling conditions were as follows: Initial denaturation at 95˚C for 3 min, followed by 40 cycles of denaturation at 95˚C for 5 sec and annealing/extension at 60˚C for 30 sec. A melting-curve analysis was subsequently performed to verify the specificity of the amplified products. The primers were designed and synthesized by Sangon Biotech Co., Ltd., and their sequences are listed in Table I. The final mRNA expression levels were calculated using the $2^{-\Delta\Delta Cq}$ method (38), with GAPDH serving as the standardized internal reference control.

Pharmacological inhibitor treatment. To investigate the involvement of CXCL8/CXCR1/2 and PI3K/Akt signaling in HMGB1 nuclear-cytoplasmic translocation, pharmacological inhibition experiments were performed in LPS/IFN-γ-stimulated THP-1-derived macrophages. For inhibition of CXCR1/2 signaling, cells were pretreated with reparixin (cat. no. HY-15251; MedChemExpress) at a final concentration of 10 μM for 6 h at 37˚C with 5% CO_2 and subsequently stimulated with LPS (100 ng/ml) and IFN-γ (20 ng/ml) until the indicated time points. For inhibition of PI3K signaling, cells were pretreated with LY294002 (cat. no. HY-10108A; MedChemExpress) at a final concentration of 20 μM for 6 h at 37˚C with 5% CO_2, followed by stimulation with LPS (100 ng/ml) and IFN-γ (20 ng/ml) for the indicated durations. Untreated cells and cells stimulated with LPS/IFN-γ alone served as the control and inflammatory stimulation groups, respectively. Following treatment, nuclear and cytoplasmic protein fractions were prepared to assess the subcellular distribution of HMGB1 by western blotting. Akt pathway activation was evaluated by detecting p-Akt at Ser473 [p-Akt (Ser473)] and total Akt protein levels.

Western blotting. Nuclear, cytoplasmic and total cellular protein fractions were prepared as aforementioned. Protein concentrations were determined using the BCA quantification kit (cat. no. BL521A; Biosharp Life Sciences). Denaturation was achieved by adding 5X loading buffer and heating at 100˚C for 10 min. Equal amounts of protein (25 μg/lane) were separated

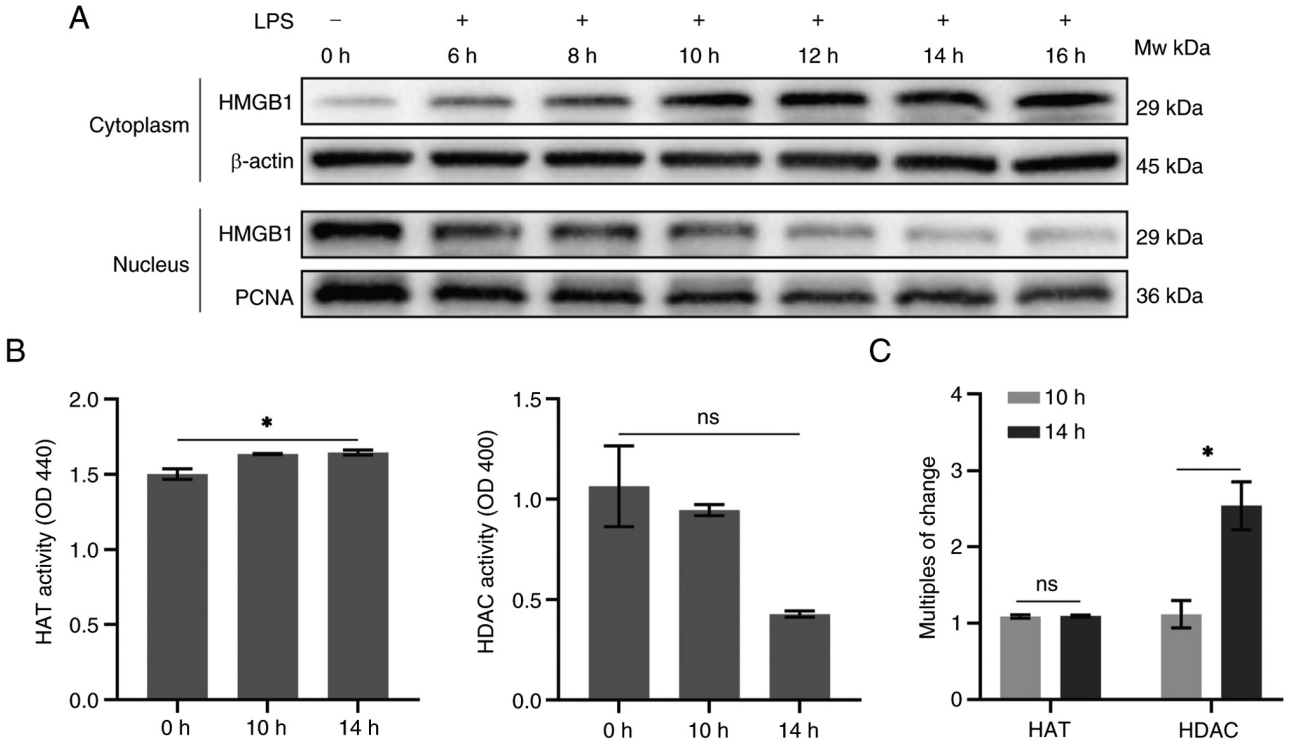


Figure 1. Intracellular expression of HMGB1, and HAT and HDAC enzyme activity in LPS-stimulated RAW264.7 cells. (A) Protein levels of HMGB1 in RAW264.7 cells were assessed using western blotting following LPS stimulation for 0, 6, 8, 10, 12, 14 and 16 h. (B) Total HAT and HDAC enzymatic activities were measured using colorimetric activity assay kits after stimulation with 100 ng/ml LPS for 10 and 14 h. (C) Fold changes in HAT and HDAC activity were calculated relative to the 0 h control group after background subtraction and normalization to protein amount. Data are presented as the mean ± SEM. *P<0.05 compared with the 0 h group (RAW264.7 cells without any treatment). All experiments were performed in triplicate. HMGB1, high mobility group box 1; HAT, histone acetyltransferase; HDAC, histone deacetylase; LPS, lipopolysaccharide; ns, no significant difference; OD, optical density; PCNA, proliferating cell nuclear antigen; Mw, molecular weight.

on 10% gels using SDS-PAGE and subsequently transferred onto PVDF membranes. The membrane was treated with 5% skimmed milk powder at room temperature for 1 h, washed three times with Tris-buffered saline containing 0.1% Tween-20 (TBST) and then incubated overnight at 4˚C with primary antibodies against HMGB1 (cat. no. 66525-1-Ig; Proteintech; 1:4,000), Akt (cat. no. 10176-2-AP; Proteintech; 1:7,000), phosphorylated (p)-Akt (Ser473; clone SY28-05; cat. no. ET1607-73; Hangzhou HuaAn Biotechnology Co., Ltd.; 1:5,000), β-actin (cat. no. 66009-1-Ig; Proteintech; 1:40,000), HRP-conjugated GAPDH (clone SA30-01; cat. no. HA724237H; Hangzhou HuaAn Biotechnology Co., Ltd.; 1:2,000), HRP-conjugated Histone H3 (clone JJ090-07; cat. no. HA724276H; Hangzhou HuaAn Biotechnology Co., Ltd.; 1:10,000) or PCNA (cat. no. 10205-2-AP; Proteintech; 1:15,000). Following washing with TBST, membranes incubated with unconjugated primary antibodies were incubated with HRP-conjugated goat anti-mouse or goat anti-rabbit IgG (cat. nos. 511103 and 511203, respectively; 1:10,000; Zen bioscience Ltd.) for 2 h at room temperature. Finally, immunoreactive bands were visualized using an enhanced chemiluminescence detection reagent (cat. no. BL520B; Biosharp Life Sciences), and chemiluminescent signals were captured using a ChemiDoc XRS imaging system (Bio-Rad Laboratories, Inc.).

Statistical analysis. All statistical analyses were performed using GraphPad Prism (version 9.0.0; Dotmatics). In the present study, cellular experiments were performed using three independent biological replicates per group (n=3). Normality was assessed using the Shapiro-Wilk test, and homogeneity of variance was assessed using Levene's test. Comparisons between two independent groups were performed using an unpaired two-tailed Student's t-test. For multiple-group comparisons, one-way ANOVA followed by Dunnett's post hoc test was used to compare each stimulated group with the corresponding 0 h or untreated control group. Analyses involving two independent factors were performed using two-way ANOVA followed by Sidak's multiple-comparisons test. P<0.05 was considered to indicate a statistically significant difference.

Results

LPS induces HMGB1 nuclear-cytoplasmic translocation and alters HAT and HDAC activities in RAW264.7 cells. To characterize the temporal dynamics of HMGB1 redistribution, nuclear and cytoplasmic HMGB1 levels were examined in RAW264.7 cells at 0, 6, 8, 10, 12, 14 and 16 h following LPS stimulation. Compared with the untreated 0 h control group, cytoplasmic HMGB1 levels increased after LPS stimulation, whereas nuclear HMGB1 levels decreased, with marked differences observed at 10 h (Fig. 1A). To determine whether these changes were accompanied by alterations in HAT and HDAC activities, total enzymatic activities were measured at 10 and 14 h. The colorimetric activity assay results demonstrated significant increases in total HAT activity at 10 and 14 h. By contrast,

total HDAC activity tended to decrease after LPS stimulation, although the differences were not statistically significant (Fig. 1B). Fold-change analysis, in which the activity values were normalized to those of the 0-h control group, showed that the magnitude of the increase in total HAT activity did not differ significantly between 10 and 14 h, whereas the magnitude of the decrease in total HDAC activity was significantly greater at 14 h than at 10 h (Fig. 1C). These findings suggest that LPS stimulation was associated with HMGB1 translocation from the nucleus to the cytoplasm and an altered HAT/HDAC enzymatic balance. However, as the assays measured total HAT and HDAC activities rather than isoform-specific enzymatic activities, the relative contributions of individual HAT and HDAC isoforms to LPS-induced HMGB1 nuclear-cytoplasmic translocation could not be determined.

Optimization of PMA-induced THP-1 cell differentiation. Representative bright-field images acquired at x100 and x200 magnification showed concentration-dependent morphological changes in THP-1 cells following PMA treatment. Treatment with 30 ng/ml PMA induced partial cellular adherence; however, attachment remained relatively weak, and only a limited proportion of cells exhibited spreading and cytoplasmic protrusions. At 100 ng/ml PMA, the majority of cells became adherent and exhibited marked spreading, pseudopodial extensions and macrophage-like morphological changes. Although treatment with 200 ng/ml PMA also induced cellular adherence and spreading, morphological features suggestive of reduced cell viability were observed. Therefore, treatment with 100 ng/ml PMA for 24 h was selected for the subsequent experiments (Fig. S1).

Cell viability under inflammatory stimulation conditions. CCK-8 assays showed that stimulation of RAW264.7 cells with 100 ng/ml LPS for 10, 12, 14 or 16 h did not significantly affect cell viability compared with the untreated control group. Similarly, stimulation of THP-1-derived macrophages with 100 ng/ml LPS and 20 ng/ml IFN-γ for the same durations did not significantly affect cell viability. These results indicated that the inflammatory stimulation conditions used in the present study did not induce substantial cytotoxicity (Fig. S2).

Screening for DEGs in sepsis and septic shock. To identify candidate genes associated with sepsis-related inflammation, differential expression analyses were performed using the GSE46955 and GSE57065 datasets. Fig. 2A and B depict centralized, stable and outlier-free data distributions. After eliminating blank, meaningless and duplicate values, a total of 999 DEGs were identified in GSE46955 (adjusted $P<0.05$; $\log_2$ FC>1), comprising 596 downregulated genes and 403 upregulated genes (Fig. 2C). In GSE57065, 768 downregulated genes and 923 upregulated genes were identified (Fig. 2D). Hierarchical cluster analysis demonstrated significant differential expression of genes in sepsis and septic shock compared with that in healthy controls, highlighting their potential association with the pathological processes of sepsis or septic shock (Fig. 2E and F).

GO and KEGG enrichment analysis. A total of 249 DEGs were identified by intersecting the GSE46955 and GSE57065 datasets using jvenn (Fig. 3A). These genes underwent functional analysis for GO gene function and KEGG pathway enrichment. GO results demonstrated significant enrichment in biological processes, including 'mononuclear cell differentiation', 'lymphocyte differentiation', 'leukocyte cell-cell adhesion', 'regulation of cell-cell adhesion', 'positive regulation of cell adhesion', 'regulation of leukocyte cell-cell adhesion', 'positive regulation of cell-cell adhesion', 'T cell differentiation', 'positive regulation of leukocyte cell-cell adhesion' and 'regulation of leukocyte apoptotic process' (Fig. 3B). Cellular component terms encompassed the 'external side of plasma membrane', 'membrane microdomain', 'membrane raft', 'secretory granule membrane', 'tertiary granule', 'specific granule', 'tertiary granule membrane', 'specific granule membrane', 'MHC protein complex' and 'MHC class II protein complex'. Molecular function terms included 'immune receptor activity', 'cytokine receptor activity', 'cytokine binding', 'MHC protein complex binding', 'G protein-coupled chemoattractant receptor activity', 'C-C chemokine binding', 'C-C chemokine receptor activity', 'RAGE receptor binding', 'MHC class II receptor activity' and 'iron ion transmembrane transporter activity' (Fig. 3B). KEGG pathway enrichment analysis revealed significant enrichment in numerous signaling pathways, including 'cytokine-cytokine receptor interaction', 'viral protein interaction with cytokine and cytokine receptor' and T helper '(Th)-1 and Th2 cell differentiation' (Fig. 3C).

Integrated network analysis identifies CXCL8 as a candidate gene. To elucidate the intricate connections among DEGs in sepsis and septic shock, a STRING analysis with a CI of 0.9 was employed. CytoNCA in Cytoscape 3.9.0 calculated degree values, pinpointing 54 key genes key in understanding the molecular landscape (Fig. 4A). A total of 381 HAT-associated targets and 936 HDAC-associated targets were obtained from GeneCards. Intersection analysis of the 54 highly connected genes, 381 HAT-associated targets and 936 HDAC-associated targets identified CXCL8 as the only gene shared among all three sets (Fig. 4B). Specifically, the values 53, 380 and 935 presented in the non-overlapping regions of Fig. 4B represent the remaining numbers of highly connected genes, HAT-associated targets and HDAC-associated targets, respectively, after excluding the shared gene CXCL8, which is displayed separately in the central overlapping region. Thus, inclusion of CXCL8 gave total set sizes of 54, 381 and 936 genes, respectively. Utilizing STRING, a comprehensive protein network centered around CXCL8 was constructed, demonstrating its intricate interactions (Fig. 4C). ROC curve analysis was performed to evaluate the discriminatory performance of CXCL8 in the discovery and validation datasets. In the discovery dataset GSE46955, CXCL8 yielded an AUC of 1.000 (95% CI, 1.000-1.000; Fig. 4D). In the other discovery dataset, GSE57065, the AUC was 0.803 (95% CI, 0.679-0.927; Fig. 4E). In the external validation dataset, GSE28750, CXCL8 yielded an AUC of 0.880 (95% CI, 0.748-1.000; Fig. 4F). To further evaluate the robustness of CXCL8, GSE69528 was incorporated as an additional external validation dataset. CXCL8 demonstrated moderate-to-good discriminatory performance in GSE69528, with an AUC of 0.801 (Fig. S3). However, as an AUC of 1.000 was observed in one dataset and may be influenced by small sample size, retrospective case-control separation and dataset-specific effects, the ROC

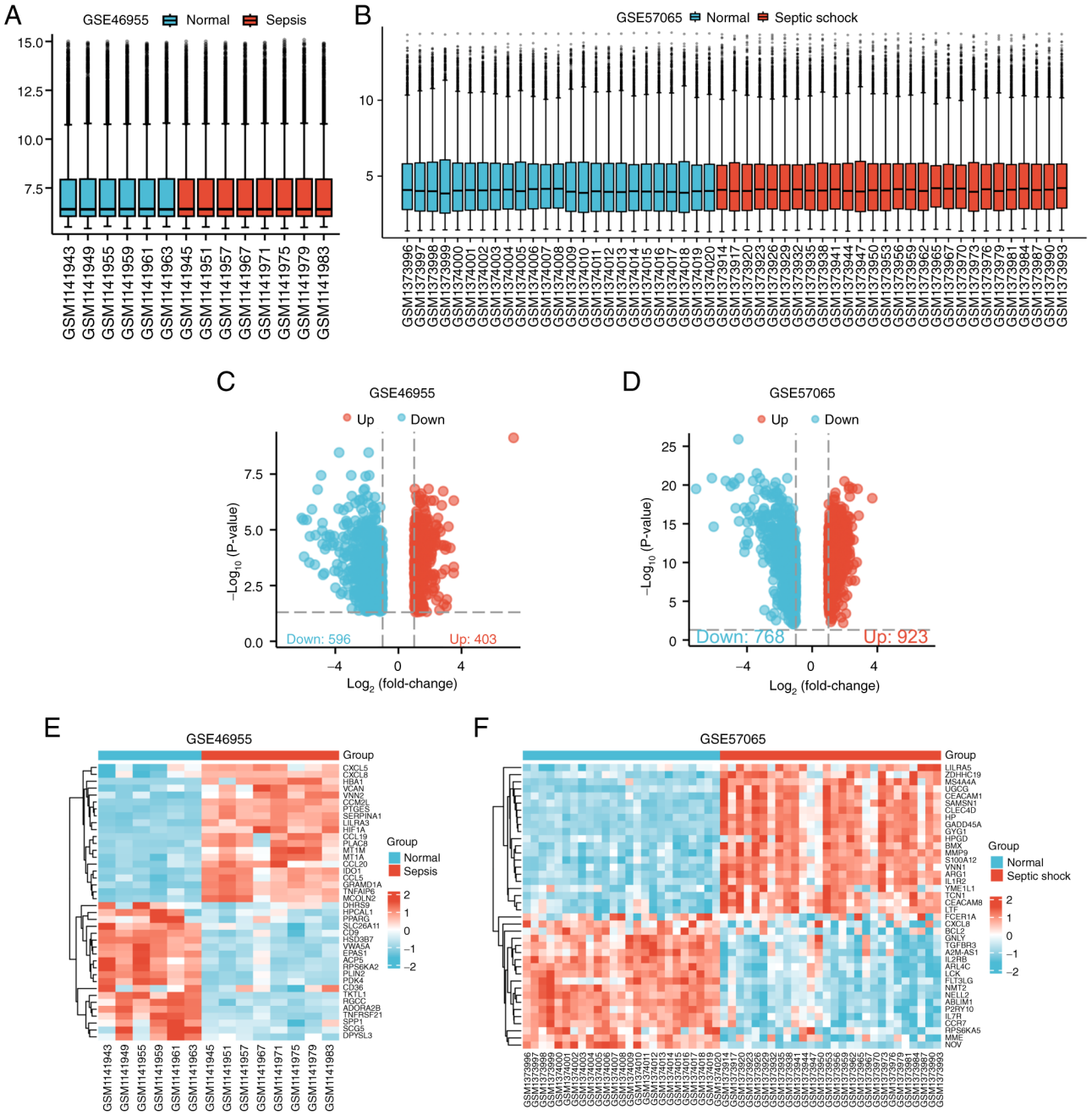


Figure 2. Screening for differentially expressed genes in sepsis and septic shock. Box plots illustrating the data distribution in (A) GSE46955 and (B) GSE57065. Volcano plots presenting the differentially expressed genes in (C) GSE46955 and (D) GSE57065. Upregulated genes are depicted in red, while downregulated genes are in blue. Bidirectional cluster analysis heatmaps of (E) GSE46955 and (F) GSE57065. Up, upregulated; Down, downregulated.

results were interpreted cautiously. Thus, CXCL8 was considered a hypothesis-generating candidate core gene rather than a clinically validated diagnostic biomarker.

Establishment of an LPS/IFN-γ-induced inflammatory macrophage model. To establish a human inflammatory macrophage model, THP-1 cells differentiated with PMA (100 ng/ml, 24 h) were stimulated with LPS (100 ng/ml) and IFN-γ (20 ng/ml). Compared with the control group, LPS/IFN-γ-stimulated cells exhibited marked morphological changes and significantly increased mRNA expression levels of TNF-α, IL-1β and IL-6, supporting the establishment of an inflammatory macrophage phenotype (Fig. 5A and B). No significant reduction in cell viability was observed under the corresponding stimulation conditions in either THP-1-derived macrophages or RAW264.7 cells (Fig. S2). Nuclear and cytoplasmic HMGB1 levels were subsequently examined at different time points after LPS/IFN-γ stimulation. Representative western blotting images indicated an overall increase in cytoplasmic HMGB1 accompanied by a decrease in nuclear HMGB1, with the reduction in nuclear HMGB1 becoming particularly evident between 10 and 16 h (Fig. 5C). These findings indicate that the HMGB1 nuclear-cytoplasmic redistribution observed in RAW264.7 cells could be reproduced in the human THP-1-derived macrophage model.

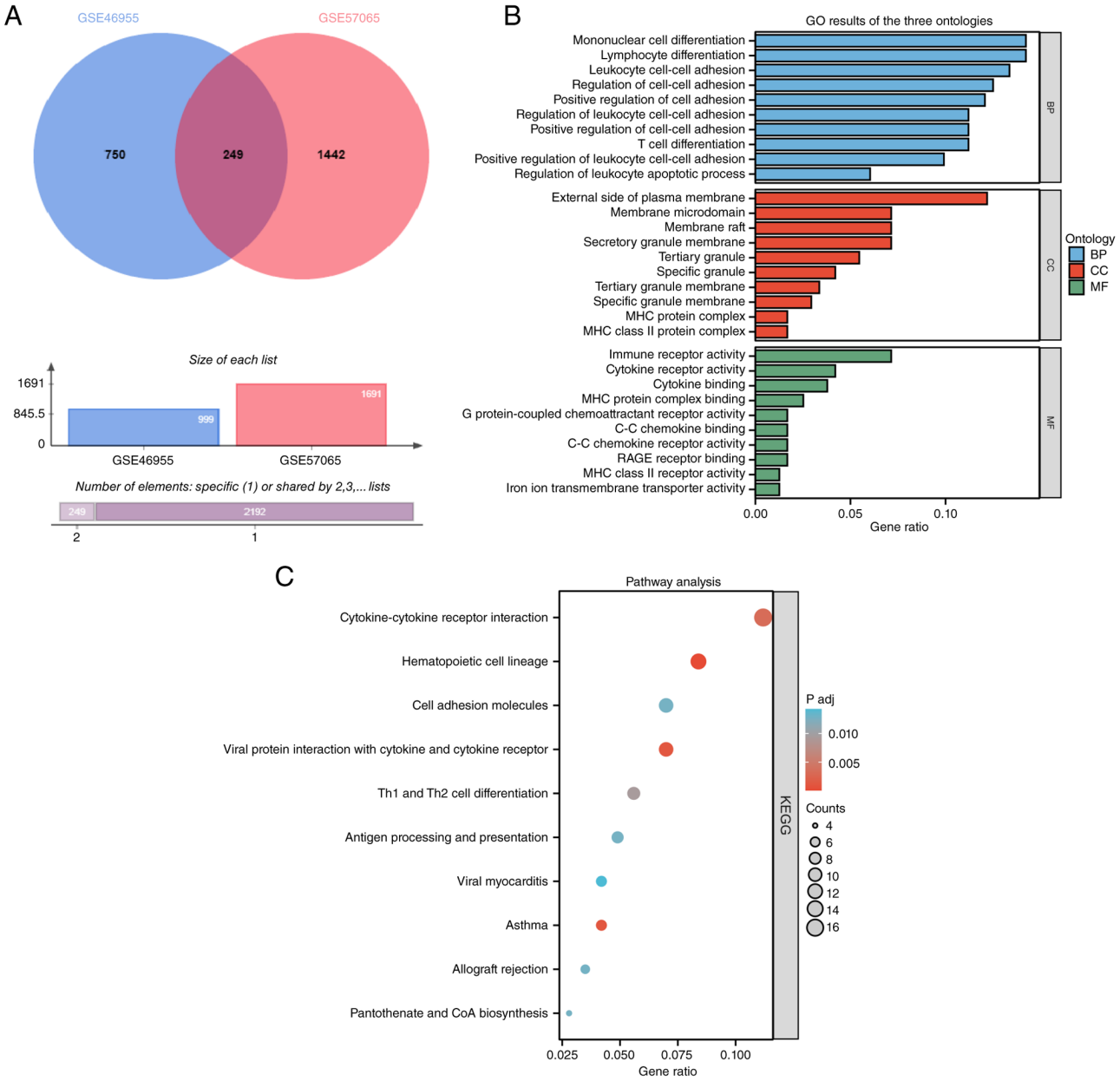


Figure 3. Enrichment analysis of 249 DEGs. (A) Venn diagram illustrating the intersection of DEGs identified from GSE46955 and GSE57065, resulting in a set of 249 genes. (B) Functional annotation through GO analysis presents the outcomes of GO enrichment analysis, categorizing the BP, CC and MF associated with the 249 DEGs. (C) KEGG enrichment analysis demonstrated the pathways significantly enriched among the 249 DEGs. The darker red color represents the more significant pathways enriched and the size of the dots represents the number of genes enriched. DEGs, differentially expressed genes; GO, Gene Ontology; BP, biological process; CC, cellular component; MF, molecular function; KEGG, Kyoto Encyclopedia of Genes and Genomes; MHC, major histocompatibility complex; RAGE, receptor for advanced glycation end-products; Th, T helper cell; adj, adjusted.

Inflammatory stimulation differentially regulates CXCL8/Akt signaling and HAT- and HDAC-associated gene expression in THP-1-derived macrophages. CXCL8 mRNA expression was assessed using RT-qPCR in LPS/IFN-γ-stimulated THP-1-derived macrophages. CXCL8 expression was found to be significantly increased after 10 and 14 h of stimulation compared with that in the control group (Fig. 6A). Western blotting demonstrated that the p-Akt (Ser473)/Akt ratio was significantly increased at 10 h compared with the 0-h control, whereas no statistically significant change was observed at 14 h (Fig. 6B and C). The expression profiles of HAT- and HDAC-associated genes were subsequently examined using RT-qPCR. The mRNA levels of CREB-binding protein (CBP) and p300, which encode transcriptional coactivators with histone acetyltransferase activity, were increased following LPS/IFN-γ stimulation (30). CBP expression demonstrated a more significant increase at 10 h, whereas the increase in p300 expression was more evident at 14 h (Fig. 6D and E). Among the HDAC isoforms assessed, HDAC1, HDAC2 and HDAC4 mRNA levels were found to be significantly decreased at 10 and/or 14 h compared with those in the 0 h control group, whereas HDAC3 demonstrated the most significant increase at 10 h, with no significant difference observed at 14 h (Fig. 6F-I). This divergent pattern indicates that HDAC3 was not uniformly downregulated with the other HDAC isoforms and therefore cannot be excluded as a potentially involved HDAC member

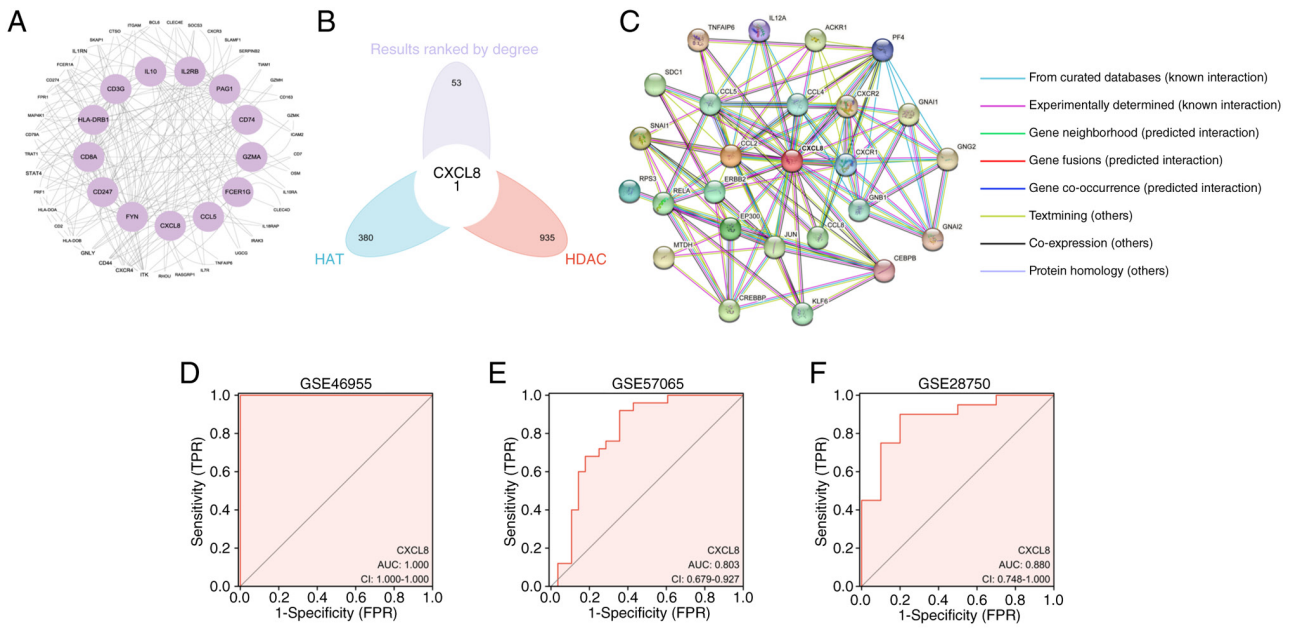


Figure 4. Protein-protein interaction network of hub genes and ROC curve analysis. (A) Protein-protein interaction network illustrating protein interactions among the 54 key genes. (B) Overlap analysis with HAT, HDAC and 54 key genes. (C) Protein network involving CXCL8. (D) ROC curve analysis of CXCL8 in GSE46955 yielded an AUC of 1.000 (CI, 1.000-1.000). (E) ROC curve analysis of CXCL8 in GSE57065 yielded an AUC of 0.803 (CI, 0.679-0.927). (F) ROC curve analysis of CXCL8 in the external validation dataset GSE28750 yielded an AUC of 0.880 (CI, 0.748-1.000). ROC, receiver operating characteristic; AUC, area under curve; HAT, histone acetyltransferase; HDAC, histone deacetylase; CXCL8, C-X-C motif chemokine ligand 8; TPR, true positive rate; FPR, false positive rate.

based on the present mRNA-level data. A comparative summary of the RT-qPCR-derived relative mRNA expression changes at 10 and 14 h showed that CBP exhibited the largest increase among the HAT-associated genes assessed, whereas HDAC4 exhibited the largest decrease among the examined HDAC isoforms (Fig. 6J). To compare the magnitudes of these changes, CBP fold-change was calculated as the expression level at each time point divided by that at 0 h, whereas HDAC4 fold change was calculated as the expression level at 0 h divided by that at each time point. The magnitude of the increase in CBP mRNA expression was significantly greater at 10 h than at 14 h, whereas the magnitude of the decrease in HDAC4 mRNA expression was significantly greater at 14 h than at 10 h (Fig. 6K).

The aforementioned findings indicate that inflammatory stimulation induced a differential transcriptional response among HAT- and HDAC-associated genes, rather than a uniform suppression of all HDAC isoforms. In particular, the divergent pattern of HDAC3 suggests that individual HDAC isoforms may be regulated in a time-dependent and isoform-specific manner under inflammatory conditions. Therefore, the present RT-qPCR data should be interpreted as changes in HAT/HDAC-associated gene expression, not as direct evidence of altered protein abundance, isoform-specific enzymatic activity or HMGB1 acetylation. In particular, the transient increase in HDAC3 mRNA suggests that HDAC3 activity cannot be ruled out without further protein-level and isoform-specific functional validation.

Pharmacological inhibition of CXCR1/2 and PI3K/Akt signaling attenuates HMGB1 nuclear-cytoplasmic translocation. To further investigate the potential involvement of CXCL8/CXCR1/2 and PI3K/Akt signaling in HMGB1 nuclear-cytoplasmic translocation, pharmacological inhibition experiments were conducted using reparixin and LY294002 in LPS/IFN-γ-stimulated THP-1-derived macrophages. Compared with untreated control cells, LPS/IFN-γ stimulation increased the cytoplasmic abundance of HMGB1 and concomitantly decreased its nuclear abundance, indicating enhanced translocation of HMGB1 from the nucleus to the cytoplasm (Fig. 7A). Pretreatment with reparixin attenuated the LPS/IFN-γ-induced accumulation of HMGB1 in the cytoplasmic fraction and increased its retention in the nuclear fraction. Pretreatment with LY294002 resulted in a similar effect on the subcellular distribution of HMGB1, with reduced cytoplasmic accumulation and increased nuclear retention following LPS/IFN-γ stimulation (Fig. 7A).

These results support the involvement of CXCL8/CXCR1/2 and PI3K/Akt signaling in inflammation-associated HMGB1 nuclear-cytoplasmic redistribution. Thus, the effects of these inhibitors on Akt signaling were subsequently examined. LPS/IFN-γ stimulation increased p-Akt (Ser473), whereas total Akt protein levels remained relatively unchanged. Pretreatment with LY294002 reduced p-Akt (Ser473; Fig. 7B). The inhibitory effect of reparixin on Akt phosphorylation further suggested that CXCR1/2 signaling may contribute to the activation of the PI3K/Akt pathway under inflammatory conditions (Fig. 7B). Collectively, these results indicate that CXCR1/2 and PI3K/Akt signaling participate in LPS/IFN-γ-induced HMGB1 nuclear-cytoplasmic translocation.

Discussion

Despite improvements in the recognition and management of clinical sepsis, the incidence and mortality rates remain

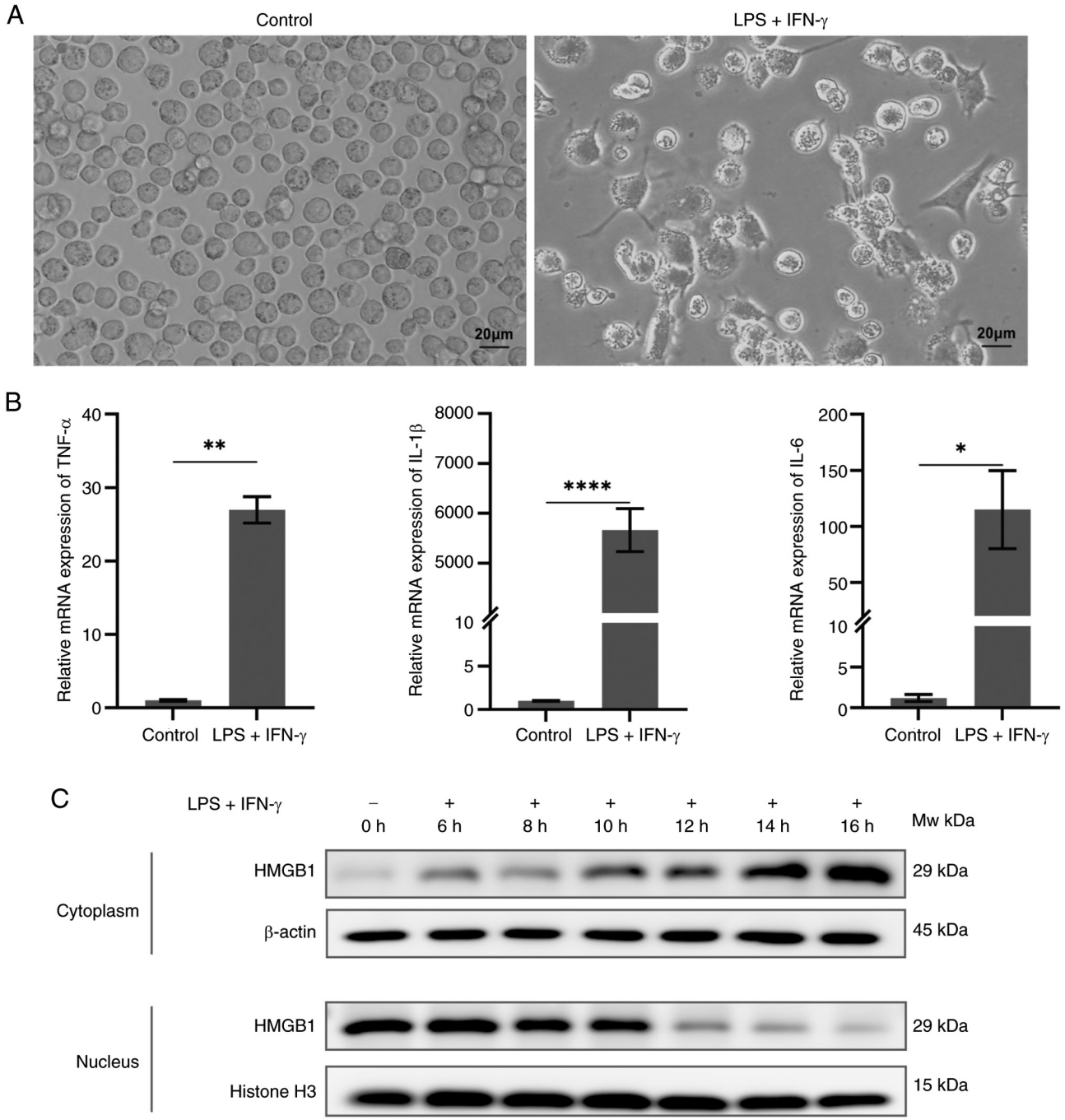


Figure 5. LPS/IFN-γ-induced inflammatory macrophage model. (A) THP-1 suspension cells were first differentiated into macrophage-like cells using treatment with 100 ng/ml phorbol 12-myristate 13-acetate for 24 h. The differentiated cells were then stimulated with 100 ng/ml LPS and 20 ng/ml IFN-γ for 10 h. Representative images show the morphological changes of THP-1-derived macrophages after inflammatory stimulation, including an elongated or spindle-like morphology (scale bar, 20 μm). (B) mRNA expression levels of TNF-α, IL-1β and IL-6 were measured using reverse transcription-quantitative PCR after 10 h of LPS/IFN-γ stimulation. Data are presented as the mean ± SEM. *P<0.05, **P<0.01 and ****P<0.0001 vs. THP-1 group (untreated). All experiments were performed in triplicate. (C) Representative western blotting images of HMGB1 in the nuclear and cytoplasmic fractions of THP-1-derived macrophages collected at 0, 6, 8, 10, 12, 14 and 16 h following stimulation with 100 ng/ml LPS and 20 ng/ml IFN-γ. β-actin and histone H3 were used as loading controls for the cytoplasmic and nuclear fractions, respectively. LPS, lipopolysaccharide; HMGB1, high mobility group box 1; Mw, molecular weight.

persistently high (39). The complexity and multifaceted nature of sepsis contributes to the difficulty in finding effective treatments. Understanding underlying mechanisms and signaling pathways is key for successful interventions. HMGB1 functions as a potent late inflammatory mediator in the pathogenesis of sepsis (17). Its translocation from the nucleus to the cytoplasm represents a key step preceding its extracellular release and subsequent pro-inflammatory activity. Although a number of mechanisms regulating this process have been reported, including JAK/STAT1-mediated HMGB1 hyperacetylation and cytoplasmic accumulation (40), the involvement of other inflammatory signaling pathways remains to be elucidated.

The present study primarily investigated the potential involvement of CXCL8/CXCR1/2-PI3K/Akt signaling in inflammation-associated HMGB1 nuclear-cytoplasmic translocation, while also examining accompanying changes

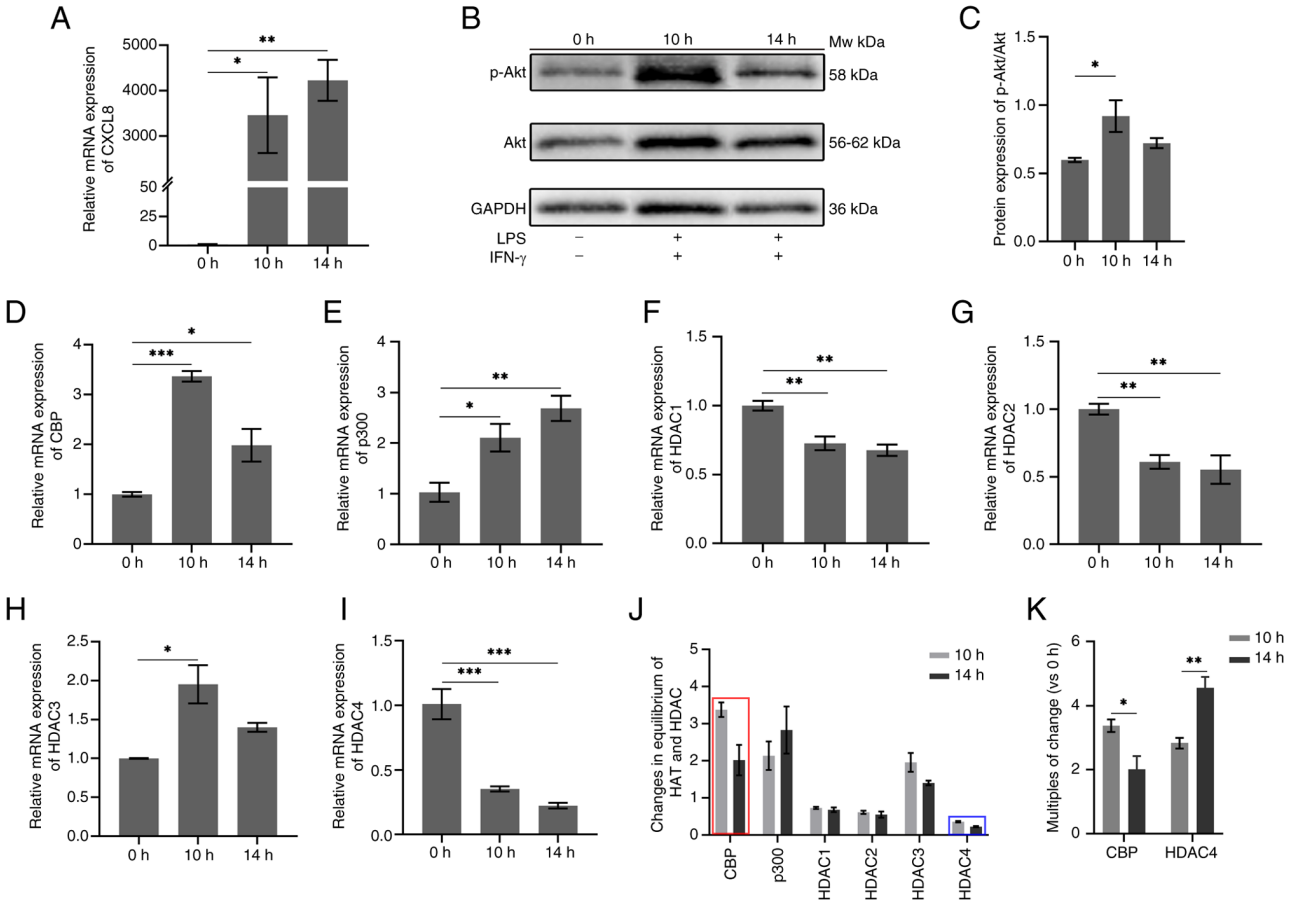


Figure 6. Validation of molecular changes in the THP-1 LPS/IFN-γ-induced inflammatory macrophage model. Reverse transcription-quantitative PCR was performed to assess alterations in CXCL8, CBP, p300 and HDAC expressions, elucidating their underlying mechanisms in the THP-1 LPS/IFN-γ-induced inflammatory macrophage model. (A) mRNA levels of CXCL8. (B) Protein levels of p-Akt (Ser473) and Akt determined using western blot analysis. (C) Quantification of p-Akt (Ser473) and Akt protein expression. mRNA levels of (D) CBP, (E) p300, (F) HDAC1, (G) HDAC2, (H) HDAC3 and (I) HDAC4. (J) Summary of relative changes in the mRNA expression levels of HAT-associated genes and HDAC isoforms after LPS/IFN-γ stimulation for 10 and 14 h. The red box indicates CBP, which demonstrated the most evident increase, whereas the blue box indicates HDAC4, which demonstrated the most evident decrease. (K) Comparison of the response magnitude of CBP and HDAC4 mRNA expression at 10 and 14 h. The y-axis represents the relative fold change in mRNA expression compared with the 0 h control group. Results are the representative mean ± SEM of three independent experiments. *P<0.05, **P<0.01 and ***P<0.001. CXCL8, C-X-C motif chemokine ligand 8; HDAC, histone deacetylase; LPS, lipopolysaccharide; HAT, histone acetyltransferase; CBP, CREB-binding protein; ns, no significant difference; p-, phosphorylated; Mw, molecular weight.

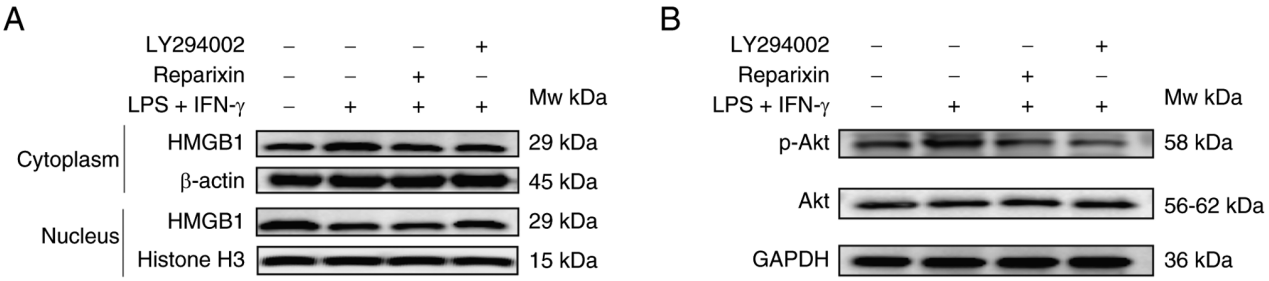


Figure 7. Pharmacological inhibition of C-X-C motif chemokine receptor-1/2 and PI3K/Akt signaling attenuates HMGB1 nuclear-cytoplasmic translocation in LPS/IFN-γ-stimulated macrophages. THP-1-derived macrophages were pretreated with reparixin (10 μM) or LY294002 (20 μM) for 6 h and subsequently stimulated with LPS (100 ng/ml) and IFN-γ (20 ng/ml) for the indicated durations. The experimental groups included untreated control cells, cells stimulated with LPS/IFN-γ, cells pretreated with reparixin followed by LPS/IFN-γ stimulation and cells pretreated with LY294002 followed by LPS/IFN-γ stimulation. (A) Representative western blotting showing HMGB1 protein levels in the cytoplasmic and nuclear fractions. β-actin and histone H3 were used as loading controls for the cytoplasmic and nuclear fractions, respectively. (B) Representative western blotting showing p-Akt (Ser473) and total Akt protein levels following pharmacological inhibitor treatment. GAPDH was used as the loading control. The results presented are representative of three independent experiments. LPS, lipopolysaccharide; HMGB1, high mobility group box 1; p-, phosphorylated; Mw, molecular weight.

in HAT/HDAC-associated molecular profiles. LPS-induced HMGB1 redistribution from the nucleus to the cytoplasm in RAW264.7 cells, and this phenomenon was reproduced in LPS/IFN-γ-stimulated THP-1-derived macrophages.

Integrated bioinformatics and experimental analyses identified CXCL8 as a candidate inflammatory mediator and demonstrated increased CXCL8 expression and Akt phosphorylation during inflammatory stimulation. Furthermore, pharmacological inhibition of CXCR1/2 or PI3K attenuated HMGB1 redistribution and reduced p-Akt. These findings provide preliminary evidence that CXCL8/CXCR1/2 and PI3K/Akt signaling participate in inflammation-associated HMGB1 nuclear-cytoplasmic translocation.

Functional enrichment analysis indicated that the shared DEGs were predominantly associated with immune cell activation and cytokine/chemokine-mediated inflammatory responses, consistent with the central role of dysregulated cytokine signaling in sepsis (41,42). Subsequent PPI and intersection analyses identified CXCL8 as the only gene shared among the 54 highly connected genes and the HAT- and HDAC-associated gene sets. This intersection did not demonstrate a direct regulatory association between CXCL8 and HATs or HDACs. Instead, it provides a bioinformatics basis for selecting CXCL8 as a candidate inflammatory mediator for subsequent investigation of the signaling mechanisms associated with HMGB1 redistribution.

CXCL8 is a key inflammatory chemokine that signals primarily through CXCR1 and CXCR2 and contributes to leukocyte recruitment and activation during infection and tissue injury (43). The elevated level of CXCL8 is considered a key contributor to sepsis development and identifies patients with sepsis with a higher risk of mortality, serving as an indicator of unfavorable prognosis (44,45). In the present study, CXCL8 mRNA expression was significantly increased in LPS/IFN-γ-stimulated THP-1-derived macrophages. ROC analysis further demonstrated that CXCL8 expression distinguished disease samples from healthy controls across the analyzed dataset. However, the AUC of 1.000 observed in one dataset should be interpreted with caution as it may be influenced by limited sample size, retrospective case-control separation, dataset-specific effects and potential overfitting. Notably, additional validation in GSE69528 revealed a more moderate AUC value of 0.801 for CXCL8, supporting its potential relevance across datasets. Therefore, the present results support CXCL8 as a hypothesis-generating candidate for mechanistic investigation rather than a clinically validated diagnostic biomarker.

PI3K/Akt is an intracellular signaling pathway involved in macrophage activation and inflammatory responses (46). Although functional associations between PI3K/Akt signaling and HMGB1 have been reported in inflammatory disease models (47,48), whether PI3K/Akt signaling participates in inflammation-induced HMGB1 nuclear-cytoplasmic translocation remains unclear. In the present study, LPS/IFN-γ stimulation increased p-Akt (Ser473) in THP-1-derived macrophages without notably altering total Akt protein levels. Increased Akt phosphorylation occurred concurrently with CXCL8 upregulation and cytoplasmic HMGB1 accumulation, indicating an association between Akt activation and inflammation-induced HMGB1 redistribution.

Pharmacological inhibition experiments provided further functional evidence supporting the involvement of CXCR1/2 and PI3K/Akt signaling. LY294002 pretreatment reduced LPS/IFN-γ-induced Akt phosphorylation, attenuated cytoplasmic HMGB1 accumulation and partially restored its nuclear retention. The present findings provide preliminary pharmacological evidence that PI3K/Akt signaling participates in HMGB1 redistribution in the present inflammatory macrophage model. Reparixin produced comparable effects, reducing Akt phosphorylation and cytoplasmic HMGB1 accumulation while increasing nuclear HMGB1 retention. This observation suggests that CXCR1/2 activity may contribute to Akt activation and HMGB1 redistribution under inflammatory conditions. Collectively, these pharmacological findings support a functional association among CXCR1/2 activity, PI3K/Akt signaling and HMGB1 nuclear-cytoplasmic translocation.

In addition to the present signaling pathway findings, inflammatory stimulation was accompanied by changes in HAT/HDAC-associated molecular profiles. Total HAT activity increased, whereas total HDAC activity decreased, following LPS exposure in RAW264.7 cells. In THP-1-derived macrophages, LPS/IFN-γ stimulation increased the mRNA expression of the HAT-associated genes CBP and p300 and decreased that of HDAC1, HDAC2 and HDAC4. By contrast, HDAC3 demonstrated a transient increase at 10 h and no significant difference at 14 h, indicating time-dependent and isoform-specific regulation rather than uniform suppression of all HDAC isoforms.

HATs and HDACs regulate cellular acetylation and deacetylation processes and may thereby influence HMGB1 subcellular trafficking (49). Previous studies demonstrated that disruption of HDAC-mediated regulation promoted HMGB1 acetylation and release. During hepatic ischemia-reperfusion injury, decreased nuclear HDAC activity involving HDAC1 and HDAC4 was associated with HMGB1 hyperacetylation, cytoplasmic translocation and release (50). Consistently, in LPS-activated macrophages, proteasome-dependent degradation of HDAC4 increased HMGB1 acetylation and secretion, whereas HDAC4 overexpression significantly inhibited both processes (51). Changes in p300 expression and HDAC4 subcellular distribution have also been associated with HMGB1 acetylation and nuclear-cytoplasmic translocation in sepsis-associated liver injury (52). In the present study, LPS stimulation increased total HAT activity and decreased total HDAC activity in RAW264.7 cells. In THP-1-derived macrophages, inflammatory stimulation increased the mRNA expression of the HAT-associated genes CBP and p300 while decreasing that of HDAC1, HDAC2 and HDAC4. By contrast, HDAC3 displayed a distinct temporal pattern, indicating that the transcriptional regulation of individual HDAC isoforms was not uniform. Overall, these enzymatic and transcriptional changes are consistent with a shift in the cellular acetylation-deacetylation balance that may favor HMGB1 acetylation, reduce its nuclear retention and facilitate its cytoplasmic accumulation. These findings suggest that HAT/HDAC-associated changes may provide an acetylation-associated molecular context for HMGB1 redistribution during inflammatory activation. However, whether these changes are regulated by CXCL8/CXCR1/2-PI3K/Akt signaling and directly alter HMGB1 acetylation remains to be determined.

Based on the combined findings, a working model is proposed in which inflammatory stimulation increases CXCL8 expression and activates CXCR1/2- and PI3K/Akt-associated signaling, thereby potentially contributing to HMGB1

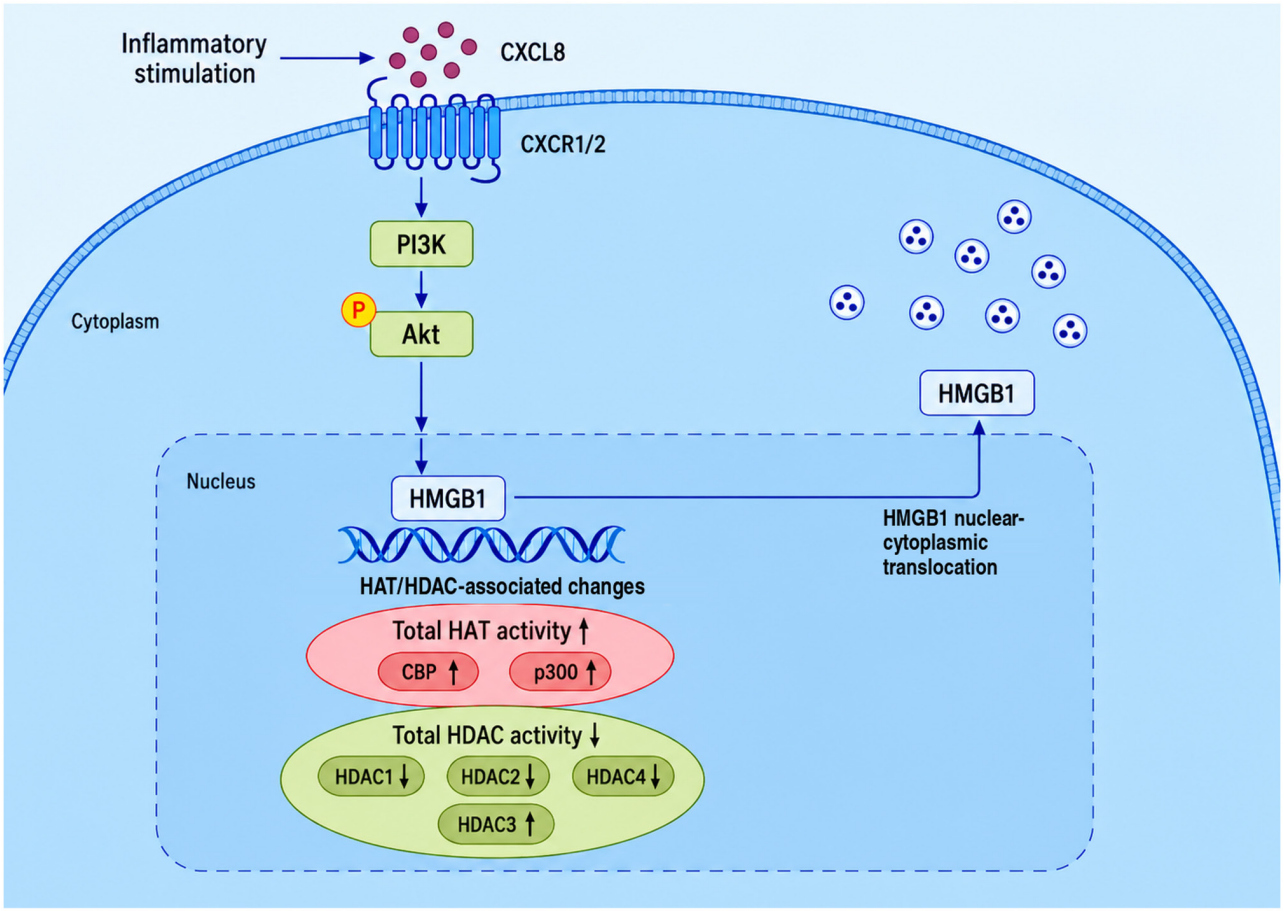


Figure 8. Proposed working model of CXCL8-associated PI3K/Akt signaling and HAT/HDAC-associated regulatory changes potentially associated with HMGB1 nuclear-cytoplasmic translocation. Figure drawn using Figdraw. CXCL8, C-X-C motif chemokine ligand 8; HDAC, histone deacetylase; HAT, histone acetyltransferase; HMGB1, high mobility group box; CXCR, CXC chemokine receptor; CBP, CREB-binding protein.

nuclear-cytoplasmic translocation (Fig. 8). Alterations in HAT/HDAC-associated activities and gene expression may accompany this signaling response and provide an additional regulatory context for HMGB1 redistribution. However, whether the HAT/HDAC-associated changes occur downstream of CXCL8/CXCR1/2-PI3K/Akt signaling and whether they directly affect HMGB1 acetylation remain to be determined.

A key limitation of the present study is that only intracellular HMGB1 nuclear-cytoplasmic redistribution was assessed in THP-1-derived macrophages. HMGB1 acetylation and total HAT/HDAC activities were not measured in this model. Notably, HMGB1 levels in culture supernatants and LDH release were not measured in the present study. Therefore, extracellular HMGB1 release and passive HMGB1 leakage resulting from membrane damage could not be evaluated. Despite the CCK-8 assays indicating no significant reduction in cell viability, this assay does not directly assess cell membrane integrity. Accordingly, the observed cytoplasmic accumulation of HMGB1 should not be interpreted as evidence of regulated HMGB1 secretion or extracellular release. Changes in CBP, p300 and HDAC mRNA expression were observed. Despite this, these transcriptional changes did not demonstrate corresponding alterations in protein abundance or isoform-specific enzymatic activity. Future studies should aim to directly measure HMGB1 acetylation in the THP-1 model. Total and isoform-specific HAT/HDAC activities should also be examined, together with the protein abundance of candidate HATs and HDACs. HMGB1 levels in culture supernatants should be quantified alongside LDH release. These measurements would help distinguish regulated extracellular release from passive leakage caused by loss of membrane integrity. Finally, the proposed framework should be evaluated in larger prospective clinical cohorts and *in vivo* sepsis models.

In conclusion, pharmacological inhibition of either CXCR1/2 or PI3K reduced Akt phosphorylation and attenuated HMGB1 nuclear-cytoplasmic translocation in LPS/IFN-γ-activated macrophages. These findings are consistent with the potential involvement of a CXCR1/2-PI3K/Akt signaling axis in HMGB1 redistribution during inflammatory macrophage activation. Further studies are required to establish the underlying molecular interactions and determine the relevance of this signaling axis to sepsis-associated inflammation.

Acknowledgements

Not applicable.

Funding

The present study was funded by the National Natural Science Foundation of China (grant no. 32201106),

the Collaborative Fund of Chengdu Medical College-Xindu District People's Hospital of Chengdu (grant no. 2021LHZD-06), the General Project of the Traditional Chinese Medicine Research Special Fund by the Sichuan Administration of Traditional Chinese Medicine (grant nos. 2024MS010 and 2024MS519), the Regional Pharmaceutical Preparation Center Joint Research Fund (Collaborative Fund of The First Affiliated Hospital of Traditional Chinese Medicine of Chengdu Medical College, XinDu Hospital of Traditional Chinese Medicine-Yingshan County Hospital of Traditional Chinese Medicine; grant no. 23LHZJ05), the Collaborative Fund of Chengdu Medical College-Nanbu People's Hospital (grant no. 23LHNBZYB08) and the Medical Research Project of Sichuan Medical Association (grant no. S2024091).

Availability of data and materials

The data generated in the present study may be requested from the corresponding author.

Authors' contributions

WC, HZ, DX and JC conceptualized and designed the present study. WC, HZ, YC and JC were responsible for the methodology. WC and HZ conducted the investigation. WC, HZ, YC, PH, YuZ, YaZ, WD and DX contributed to data acquisition and validation. CW contributed to data acquisition and analysis. WS contributed to data interpretation and critically revised the manuscript for important intellectual content. WC, HZ and YC curated the present data and prepared the original manuscript draft. JC supervised the study. WC and HZ confirm the authenticity of all the raw data. All authors critically reviewed the manuscript for important intellectual content. All authors have read and approved the final version of the manuscript.

Ethics approval and consent to participate

Not applicable.

Patient consent for publication

Not applicable.

Competing interests

The authors declare that they have no competing interests.

References

1. Singer M, Deutschman CS, Seymour CW, Shankar-Hari M, Annane D, Bauer M, Bellomo R, Bernard GR, Chiche JD, Coopersmith CM, *et al*: The Third International consensus definitions for sepsis and septic shock (Sepsis-3). JAMA 315: 801-810, 2016.
2. Cheng Z, Abrams ST, Toh J, Wang SS, Wang Z, Yu Q, Yu W and Toh Chand Wang G: The critical roles and mechanisms of immune cell death in sepsis. Front Immunol 11: 1918, 2020.
3. Liu D, Huang SY, Sun JH, Zhang HC, Cai QL, Gao C, Li L, Cao J, Xu F, Zhou Y, *et al*: Sepsis-induced immunosuppression: mechanisms, diagnosis and current treatment options. Mil Med Res 9: 56, 2022.
4. Rudd KE, Johnson SC, Agesa KM, Shackelford KA, Tsoi D, Kievlan DR, Colombara DV, Ikuta KS, Kissoon N, Finfer S, *et al*: Global, regional, and national sepsis incidence and mortality, 1990-2017: Analysis for the Global Burden of disease study. Lancet 395: 200-211, 2020.
5. Weng L, Xu Y, Yin P, Wang Y, Chen Y, Liu W, Li S, Peng JM, Dong R, Hu XY, *et al*: National incidence and mortality of hospitalized sepsis in China. Crit Care 27: 84, 2023.
6. Deng M, Tang Y, Li W, Wang X, Zhang R, Zhang X, Zhao X, Liu J, Tang C, Liu Z, *et al*: The endotoxin delivery protein HMGB1 mediates caspase-11-dependent lethality in sepsis. Immunity 49: 740-753 e747, 2018.
7. He C, Sun S, Zhang Y, Xie F and Li S: The role of irreversible electroporation in promoting M1 macrophage polarization via regulating the HMGB1-RAGE-MAPK axis in pancreatic cancer. Oncoimmunology 10: 1897295, 2021.
8. Kang R, Chen R, Zhang Q, Hou W, Wu S, Cao L, Huang J, Yu Y, Fan XG, Yan Z, *et al*: HMGB1 in health and disease. Mol Aspects Med 40: 1-116, 2014.
9. Andersson U and Yang H: HMGB1 is a critical molecule in the pathogenesis of Gram-negative sepsis. J Intensive Med 2: 156-166, 2022.
10. Deng M, Scott MJ, Fan J and Billiar TR: Location is the key to function: HMGB1 in sepsis and trauma-induced inflammation. J Leukoc Biol 106: 161-169, 2019.
11. Chen R, Kang R and Tang D: The mechanism of HMGB1 secretion and release. Exp Mol Med 54: 91-102, 2022.
12. Gao SQ, Zhang H, He JG, Zheng HL, Zhang PW, Xu JF, Shen ZC, Zhao HH, Wang F, Hu ZL and Chen JG: Neuronal HMGB1 in nucleus accumbens regulates cocaine reward memory. Addict Biol 25: e12739, 2020.
13. Sunden-Cullberg J, Norrby-Teglund A, Rouhiainen A, Rauvala H, Herman G, Tracey KJ, Lee ML, Andersson J, Tokics L and Treutiger CJ: Persistent elevation of high mobility group box-1 protein (HMGB1) in patients with severe sepsis and septic shock. Crit Care Med 33: 564-573, 2005.
14. Karkischenko VN, Skvortsova VI, Gasanov MT, Fokin YV, Nesterov MS, Petrova NV, Alimkina OV and Pomytkin IA: Inhaled [D-Ala(2)]-dynorphin 1-6 prevents hyperacetylation and release of high mobility group box 1 in a mouse model of acute lung injury. J Immunol Res 2021: 4414544, 2021.
15. Lamkanfi M, Sarkar A, Vande Walle L, Vitari AC, Amer AO, Wewers MD, Tracey KJ, Kanneganti TD and Dixit VM: Inflammasome-dependent release of the alarmin HMGB1 in endotoxemia. J Immunol 185: 4385-4392, 2010.
16. Lu B, Nakamura T, Inouye K, Li J, Tang Y, Lundbäck P, Valdes-Ferrer SI, Olofsson PS, Kalb T, Roth J, *et al*: Novel role of PKR in inflammasome activation and HMGB1 release. Nature 488: 670-674, 2012.
17. Wang H, Bloom O, Zhang M, Vishnubhakat JM, Ombrellino M, Che J, Frazier A, Yang H, Ivanova S, Borovikova L, *et al*: HMG-1 as a late mediator of endotoxin lethality in mice. Science 285: 248-251, 1999.
18. Xue J, Suarez JS, Minaai M, Li S, Gaudino G, Pass HI, Carbone M and Yang H: HMGB1 as a therapeutic target in disease. J Cell Physiol 236: 3406-3419, 2021.
19. Qi X, Wang H, Xia L, Lin R, Li T, Guan C and Liu T: miR-30b-5p releases HMGB1 via UBE2D2/KAT2B/HMGB1 pathway to promote pro-inflammatory polarization and recruitment of macrophages. Atherosclerosis 324: 38-45, 2021.
20. Zhou X, Qiu Y, Mu K and Li Y: Decreased SIRT1 protein may promote HMGB1 translocation in the keratinocytes of patients with cutaneous lupus erythematosus. Indian J Dermatol Venereol Leprol 1-8, 2023 (Epub ahead of print).
21. Yin J, Liu F, Xia H, Yan S, Wang Y, Li X, Shi Y, Wang Y, Jing Y, Li Y and Hu H: P300-targeted acetylome reveals a role for HMGB1 translocation in central cardiac sympathetic activation post myocardial infarction. J Inflamm Res 18: 15329-15347, 2025.
22. De-Leon-Lopez YS, Thompson ME, Kean JJ and Flaherty RA: The PI3K-Akt pathway is a multifaceted regulator of the macrophage response to diverse group B Streptococcus isolates. Front Cell Infect Microbiol 13: 1258275, 2023.
23. Palombo R, Passacantilli I, Terracciano F, Capone A, Matteocci A, Tournier S, Alberdi A, Chiurchiù V, Volpe E and Paronetto MP: Inhibition of the PI3K/AKT/mTOR signaling promotes an M1 macrophage switch by repressing the ATF3-CXCL8 axis in Ewing sarcoma. Cancer Lett 555: 216042, 2023.

24. Oh YJ, Youn JH, Min HJ, Kim DH, Lee SS, Choi IH and Shin JS: CKD712, (S)-1-(α-naphthylmethyl)-6,7-dihydroxy-1,2,3,4-tetrahydroisoquinoline, inhibits the lipopolysaccharide-stimulated secretion of HMGB1 by inhibiting PI3K and classical protein kinase C. Int Immunopharmacol 11: 1160-1165, 2011.
25. Shao Y, Lan Y, Chai X, Gao S, Zheng J, Huang R, Shi Y, Xiang Y, Guo H, Xi Y, *et al*: CXCL8 induces M2 macrophage polarization and inhibits CD8(+) T cell infiltration to generate an immunosuppressive microenvironment in colorectal cancer. FASEB J 37: e23173, 2023.
26. Park SE, Park K, Kim E, Kim CY, Hwang SM, Lee JM, Suh JY, Lee Y, Kim MO and Kim YG: CXCL5/CXCL8 induces neutrophilic inflammation in peri-implantitis. J Periodontal Res 59: 698-711, 2024.
27. Meng ZW, Zhang L, Cai XR, Wang X, She FF and Chen YL: IL-8 is a novel prometastatic chemokine in intrahepatic cholangiocarcinoma that induces CXCR2-PI3K/AKT signaling upon CD97 activation. Sci Rep 13: 18711, 2023.
28. Wang L, Zhu L, Duan C, Li L and Chen G: Total saponin of Dioscorea collettii attenuates MSU crystal-induced inflammation via inhibiting the activation of the NALP3 inflammasome and caspase-1 in THP-1 macrophages. Mol Med Rep 21: 2466-2474, 2020.
29. Cho HY, Ahn S, Cho YS, Seo SK, Kim DH, Shin JG and Lee SJ: CYP2C19 Contributes to THP-1-Cell-Derived M2 macrophage polarization by producing 11,12- and 14,15-epoxyeicosatrienoic acid, agonists of the PPARγ receptor. Pharmaceuticals (Basel) 16: 593, 2023.
30. Shalova IN, Lim JY, Chittezhath M, Zinkernagel AS, Beasley F, Hernández-Jiménez E, Toledano V, Cubillos-Zapata C, Rapisarda A, Chen J, *et al*: Human monocytes undergo functional re-programming during sepsis mediated by hypoxia-inducible factor-1α. Immunity 42: 484-498, 2015.
31. Cazalis MA, Lepape A, Venet F, Frager F, Mougin B, Vallin H, Paye M, Pachot A and Monneret G: Early and dynamic changes in gene expression in septic shock patients: A genome-wide approach. Intensive Care Med Exp 2: 20, 2014.
32. Wickham H: ggplot2: Elegant Graphics for Data Analysis. Springer-Verlag New York, New York, NY, 2016.
33. Ritchie ME, Phipson B, Wu D, Hu Y, Law CW, Shi W and Smyth GK: Limma powers differential expression analyses for RNA-sequencing and microarray studies. Nucleic Acids Res 43: e47, 2015.
34. Gu Z, Eils R and Schlesner M: Complex heatmaps reveal patterns and correlations in multidimensional genomic data. Bioinformatics 32: 2847-2849, 2016.
35. Wu T, Hu E, Xu S, Chen M, Guo P, Dai Z, Feng T, Zhou L, Tang W, Zhan L, *et al*: clusterProfiler 4.0: A universal enrichment tool for interpreting omics data. Innovation (Camb) 2: 100141, 2021.
36. Shannon P, Markiel A, Ozier O, Baliga NS, Wang JT, Ramage D, Amin N, Schwikowski B and Ideker T: Cytoscape: A software environment for integrated models of biomolecular interaction networks. Genome Res 13: 2498-2504, 2003.
37. Robin X, Turck N, Hainard A, Tiberti N, Lisacek F, Sanchez JC and Müller M: pROC: An open-source package for R and S+ to analyze and compare ROC curves. BMC Bioinformatics 12: 77, 2011.
38. Livak KJ and Schmittgen TD: Analysis of relative gene expression data using real-time quantitative PCR and the 2(-Delta Delta C(T)) Method. Methods 25: 402-408, 2001.
39. Cecconi M, Evans L, Levy M and Rhodes A: Sepsis and septic shock. Lancet 392: 75-87, 2018.
40. Lu B, Antoine DJ, Kwan K, Lundbäck P, Wähämaa H, Schierbeck H, Robinson M, Van Zoelen MA, Yang H, Li J, *et al*: JAK/STAT1 signaling promotes HMGB1 hyperacetylation and nuclear translocation. Proc Natl Acad Sci USA 111: 3068-3073, 2014.
41. Liang P, Wu Y, Qu S, Younis M, Wang W, Wu Z and Huang X: Exploring the biomarkers and potential therapeutic drugs for sepsis via integrated bioinformatic analysis. BMC Infect Dis 24: 32, 2024.
42. Lu L, Liu LP, Gui R, Dong H, Su YR, Zhou XH and Liu FX: Discovering common pathogenetic processes between COVID-19 and sepsis by bioinformatics and system biology approach. Front Immunol 13: 975848, 2022.
43. Cambier S, Gouwy M and Proost P: The chemokines CXCL8 and CXCL12: Molecular and functional properties, role in disease and efforts towards pharmacological intervention. Cell Mol Immunol 20: 217-251, 2023.
44. Bozza FA, Salluh JI, Japiassu AM, Soares M, Assis EF, Gomes RN, Bozza MT, Castro-Faria-Neto HC and Bozza PT: Cytokine profiles as markers of disease severity in sepsis: A multiplex analysis. Crit Care 11: R49, 2007.
45. Anderson BJ, Calfee CS, Liu KD, Reilly JP, Kangelaris KN, Shashaty MGS, Lazaar AL, Bayliffe AI, Gallop RJ, Miano TA, *et al*: Plasma sTNFR1 and IL8 for prognostic enrichment in sepsis trials: A prospective cohort study. Crit Care 23: 400, 2019.
46. Vergadi E, Ieronymaki E, Lyroni K, Vaporidi K and Tsatsanis C: Akt signaling pathway in macrophage activation and M1/M2 polarization. J Immunol 198: 1006-1014, 2017.
47. Kim JH, Kim SJ, Lee IS, Lee MS, Uematsu S, Akira S and Oh KI: Bacterial endotoxin induces the release of high mobility group box 1 via the IFN-beta signaling pathway. J Immunol 182: 2458-2466, 2009.
48. Li R, Zou X, Huang H, Yu Y, Zhang H, Liu P, Pan S, Ouyang Y and Shang Y: HMGB1/PI3K/Akt/mTOR signaling participates in the pathological process of acute lung injury by regulating the maturation and function of dendritic cells. Front Immunol 11: 1104, 2020.
49. Bonaldi T, Talamo F, Scaffidi P, Ferrera D, Porto A, Bachi A, Rubartelli A, Agresti A and Bianchi ME: Monocytic cells hyperacetylate chromatin protein HMGB1 to redirect it towards secretion. EMBO J 22: 5551-5560, 2003.
50. Evankovich J, Cho SW, Zhang R, Cardinal J, Dhupar R, Zhang L, Klune JR, Zlotnicki J, Billiar T and Tsung A: High mobility group box 1 release from hepatocytes during ischemia and reperfusion injury is mediated by decreased histone deacetylase activity. J Biol Chem 285: 39888-39897, 2010.
51. Park EJ, Kim YM, Kim HJ and Chang KC: Degradation of histone deacetylase 4 via the TLR4/JAK/STAT1 signaling pathway promotes the acetylation of high mobility group box 1 (HMGB1) in lipopolysaccharide-activated macrophages. FEBS Open Bio 8: 1119-1126, 2018.
52. Tian T, Yao D, Zheng L, Zhou Z, Duan Y, Liu B, Wang P and Li Y: Sphingosine kinase 1 regulates HMGB1 translocation by directly interacting with calcium/calmodulin protein kinase II-δ in sepsis-associated liver injury. Cell Death Dis 11: 1037, 2020.

Copyright © 2026 Chen et al. This work is licensed under a Creative Commons Attribution-NonCommercial-NoDerivatives 4.0 International (CC BY-NC-ND 4.0) License.